Effects of Virtual Resistance on Transient Stability of Virtual Synchronous Generators under Grid Voltage Sag

Xiong, Xiaoling; Wu, Chao; Blaabjerg, Frede

Published in:
IEEE Transactions on Industrial Electronics

DOI (link to publication from Publisher):
10.1109/TIE.2021.3082055

Publication date:
2022

Document Version
Accepted author manuscript, peer reviewed version

Effects of Virtual Resistance on Transient Stability of Virtual Synchronous Generators under Grid Voltage Sag

Xiaoling Xiong, *Member*, *IEEE*, Chao Wu, *Member*, *IEEE*, and Frede Blaabjerg, *Fellow*, *IEEE*,

***Abstract*—The virtual synchronous generator (VSG) control of a grid-connected converter is an attractive interfacing solution for high-penetration renewable generation systems. Unfortunately, the synchronous resonance (SR) can appear due to the power control loops, which are usually damped by adopting a virtual resistance (VR). However, the effects of VR on the transient stability of the VSG are rarely studied. A virtual point of common coupling and a virtual power angle concept is proposed in this paper to represent the mathematical model of the VSG with VR damping. Based on the model, the transient stability is further analyzed using the phase portrait and the attraction regions of the nonlinear system. It reveals that the VR has a negative and different impact on transient stability, compared with the real grid resistor. In order to keep the VSG with VR to work normally during the grid voltage sag, an enhanced transient stability method, by reducing the active power commands when the grid fault is detected, is introduced. A design-oriented analysis and the parameter design with different VRs are also presented. Finally, the theoretical analysis is verified by experimental results.**

***Index Terms*—Virtual synchronous generators (VSGs), transient stability, virtual resistance, synchronous frequency resonance.**

I. Introduction

Over the past decades, more and more distributed renewable energy sources are connected to the conventional power grid, using voltage source converters (VSCs) as the interface [1]-[5]. The majority of the grid-connected VSCs are designed to operate in parallel with the conventional grid, which transfers their collected power to the grid under the constraint of grid codes. Grid-following converters can effectively control the current injected into the grid and ride through most grid faults. However, they can not operate in the standalone mode and may have stability problems when connected to a weak grid since their control is dependent on the voltage synchronization based on a phase-locked loop [2], [3]. Therefore, to avoid the shortcomings of the grid-following converters, grid-forming converters, inspired from the operation of synchronous generators (SGs), have been developed quickly and gained more and more attention [4], [5]. The grid-forming converters can generally provide voltage support, and they can operate in both grid-connected and standalone modes with minor changes in control.

Since the penetration of converter-based renewable energy resources is continuously growing, the existing power grid becomes weaker, i.e., the short circuit ratio (SCR) is becoming lower. As the ratio of SGs based generation decreases, the inertia of the power grid is reduced [6], which will jeopardize the frequency stability during the grid transients [7]. In order to provide inertia support for the grid, like the SGs, the concept of the virtual synchronous generators (with various names such as VSG, virtual synchronous machine, synchronverter, etc.) has been reported in [8]-[12]. In this paper, for the sake of convenience, all these similar control methods are referred to as VSG, which intends to mimic the swing equation of an SG in a converter and emulate the kinetic energy of a rotating mass by adding a short term energy storage. As one of the grid-forming control strategies, VSG controlled converter can support both voltage and frequency simultaneously.

In addition to frequency and voltage support, the VSG can also improve the small-signal stability of the multi-converter system under a weak grid [13], [14]. However, the integration of VSGs will inevitably influence the low-frequency oscillations (LFOs) in power grids, which are usually caused by the interactions among different VSGs. In order to mitigate the LFOs, a parameter alternating VSG controller is proposed by changing the inertia and droop coefficients flexibility [15]. In [16], a positive damping torque method is presented for damping the LFOs. Besides the LFOs caused by the integration of VSGs, there may also be subsynchronous resonance (SSR) when VSG is connected to a series-compensated grid. The virtual impedance method is introduced for suppressing the SSR in [17], [18]. Despite the LFOs and SSR, several investigations have shown that synchronous resonance (SR) is another typical instability of the grid-connected VSG, which inherently exists in the power control loop [19]-[23]. By adding a real resistor to the output of the converter, the grid resistance

Manuscript received November 27, 2020; revised January 28, 2021 and April 15, 2021; accepted May 10, 2021. This work is supported by the National Natural Science Foundation of China under Grant 51707065 and part by THE VELUX FOUNDATIONS under the VILLUM Investigator Grant REPEPS (Award Ref. No.: 00016591) (*Corresponding author: Chao Wu*).

Xiaoling Xiong is with the School of Electrical & Electronic Engineering, North China Electric Power University, Beijing, 102206, China (e-mail: xiongxl1102@ncepu.edu.cn).

Chao Wu and Frede Blaabjerg are with the Department of Energy Technology, Aalborg University, Aalborg 9220, Denmark (e-mail: cwu@et.aau.dk and fbl@et.aau.dk).

This article has been accepted for publication in a future issue of this journal, but has not been fully edited. Content may change prior to final publication. Citation information: DOI 10.1109/TIE.2021.3082055, IEEE Transactions on Industrial Electronics

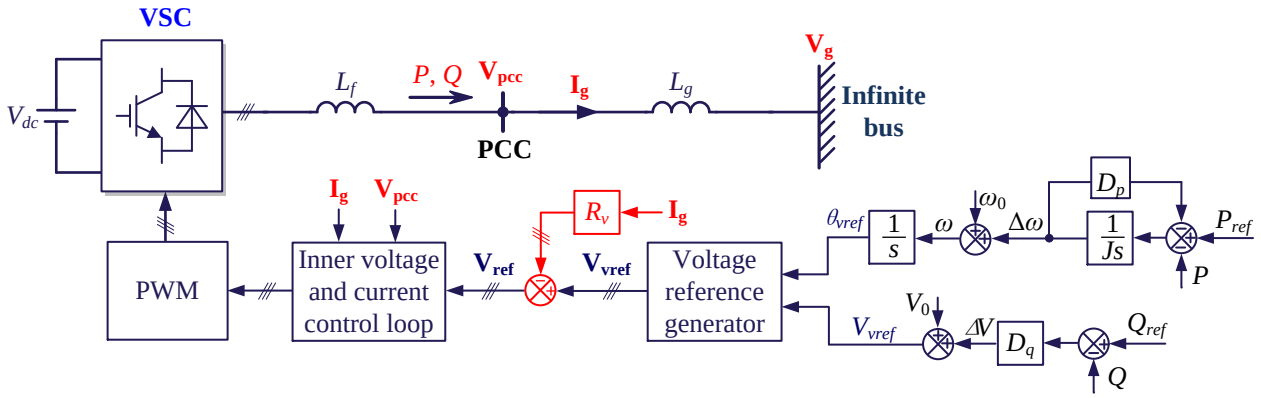

Fig. 1. General topology and control scheme of a three-phase grid-connected VSG using the virtual resistance damping.

can be equivalently increased, which is able to dampen the SR. Still, it causes extra loss and reduces system efficiency. Especially in the high-voltage power grid, the inductive line impedance is typically much higher than the resistive one, where the resistance can be neglected without making any significant error [24]. Thus, the virtual resistance (VR) is inevitably employed in the control loop and inserted into line impedance so that the SR can be suppressed without introducing any power loss. However, most of the research is only focused on the small-signal analysis of the VSG. For illustration, the VR properties, and the selection recommendation have been studied in detail from a small-signal stability perspective over the years [20]-[23]. Yet, the effects of VR on large-signal transient stability are rarely studied.

In contrast to the small-signal stability analysis, only a few studies on transient stability of the VSG, i.e., the ability of the VSG to maintain synchronization with the grid when subjected to a large disturbance [25]-[29], have been reported. In [25], it has been found there is a conflict between the frequency response and the transient stability, indicating large inertia may drive the VSG to lose stability during a large disturbance. A transient damping control method is proposed in [26] based on Lyapunov's direct method. The transient stability can be enhanced, but the design method for the additional damping coefficient is absent. A mode-switching control method is further reported in [27] for riding through the grid voltage sag by changing the VSG mode during the grid faults. However, the mode detection block uses a differentiation element, which may cause a lot of noise and unexpected system instability. Thus, it is challenging to be implemented in practice. Meanwhile, there will be oscillation within a hysteresis boundary when the VSG didn't have an equilibrium point after the grid voltage sag by using the mode-switching control method. The transient stability of a single-loop voltage-magnitude (SLVM) controlled VSG is analyzed in [28]. It was found that the voltage reference of the point of common coupling (PCC) is not ideally tracked in such a control scheme. The output filter L_f must be considered in SLVM control, which will reduce the power transfer capability, indicating a negative impact on transient stability. Moreover, the overcurrent limitation can not be embedded as there is no inner current loop. The authors in [29] overview the grid-synchronization stability of the converter-based resources, including the VSG control. However, all of these studies overlooked the effects of VR on transient stability.

This paper is going to fill this gap, and the main contributions can be summarized as

1. A virtual PCC and a virtual power angle are proposed to derive the mathematical model of the VSG with VR damping. Differing from the grid resistance, VR is implemented in control and equivalently appears before the PCC, rather than after the PCC. Consequently, the effects of the VR are different from the grid resistance, which is modeled based on the virtual PCC and virtual power angle.

2. The transient stability is analyzed using the phase portrait and the attraction regions of the VSG with VR damping. It reveals that the impacts of VR on transient stability are opposite from the grid resistance, which narrowed the VSG's stability region, resulting in reducing the active power transfer capability.

3. In order to keep the VSG work normally during the grid voltage sag, an improved method, by reducing the active power reference commands when the grid fault is detected, is introduced to enhance the transient stability. A design-oriented analysis and the parameter design with different VRs are also presented based on the phase portrait of the VSG.

This paper is organized as follows. The VSG configuration and SR phenomena are presented in Section II. The virtual PCC and virtual power angle are proposed in Section III. The effects of the VR on transient stability are studied and revealed by the phase portrait analysis and the attraction region of the nonlinear system. Section IV introduces a transient stability enhancement method by reducing the active power reference during the grid voltage sag to avoid the negative impacts. Detailed parameter design guidelines of the coefficient parameters are also presented. The theoretical analysis is verified in Section V by experimental results, and the conclusion is drawn in Section VI.

II. A GLIMPSE OF THE VSG SYSTEM AND SR PHENOMENA

A. *The VSG System Description*

Fig. 1 shows the general topology and control scheme of a grid-connected VSG, including the VR for active damping. A three-phase converter is connected to the traditional power grid

at the PCC through an inductor filter L_f. The grid is modeled as an infinite bus connected in series with an impedance [19], [21], i.e., an inductance L_g and a resistor R_g. $\mathbf{V_g}=V_g e^{j\omega_g t}$ is the space vector of the grid voltage, where ω_g usually is equal to the synchronous angular frequency ω_0. $\mathbf{V_{pcc}}=V_{pcc}e^{j\theta_{pcc}}$ and $\mathbf{I_g}$ represents the voltage and current space vectors of the PCC voltage and current, respectively, where θ_{pcc} is the PCC voltage phase. P and Q represent the active and reactive power injected into the grid from the PCC. Generally, a large capacitor is used on the dc side, or energy storage is employed to make an inertia contribution, where the dc voltage is taken over by the front-end converter [19] or by the energy storage converter [30]. Hence, constant dc-link voltage is adopted in this paper when studying the transient stability of the VSG as in [25], [27]-[29].

As shown in Fig. 1, P_{ref} and Q_{ref} are the active and reactive power references, respectively. The power control is implemented with VSG control to generate the PCC voltage reference, i.e., $\mathbf{V_{vref}}=V_{vref}e^{j\theta_{vref}}$. R_v is the VR for active damping, which is used to suppress the synchronous resonance of VSG [19]-[23]. The PCC voltage reference is changed to $\mathbf{V_{ref}}$, given as $\mathbf{V_{ref}}=\mathbf{V_{vref}}-R_v\mathbf{I_g}$.Usually, inner voltage and current control loops are employed to force $\mathbf{V_{pcc}}$ to track the reference and provide overcurrent protection with limiting the current reference. It should be noted that the outer power control loop mainly determines the transient stability because the bandwidth of the inner loop is usually designed much higher than that of the outer power control loops [2]. Thus, the inner control loop can be regarded as one during the transient stability analysis. Due to the decoupled timescales, an ideal voltage reference tracking is assumed, i.e., $\mathbf{V_{pcc}}=\mathbf{V_{ref}}$. If a severe grid fault occurs, resulting in the overcurrent protection is triggered, the control scheme should be changed to grid-following control. Under this condition, the transient stability problems are mainly caused by PLL, which has been studied and explained in [31]. Thus, this paper only focuses on the VSG's transient stability under a light grid voltage sag, which won't trigger the overcurrent protection.

To implement the VSG control scheme, the active power control loop is used to adjust the phase of the PCC voltage reference, i.e., θ_{vref}, by emulating the swing equation of the SG, as shown in Fig. 1. ω is the angular frequency of the VSG, and $\omega=\omega_0+\Delta\omega$, which can be derived from Fig. 1, given in the complex frequency domain with Laplace transformation as

$$\omega(s)=\omega_0(s)+\frac{1}{Js+D_p}\cdot\left(P_{ref}(s)-P(s)\right) \tag{1}$$

where J and D_p are the virtual inertia and droop gain of frequency governor. $\omega(s)$, $\omega_0(s)$, $P_{ref}(s)$ and $P(s)$ are the Laplace transformed variables of ω, ω_0, P_{ref} and P, respectively.

The reactive power-voltage (Q-V) droop control is adopted for the reactive power control, which is used to regulate V_{vref}, where the control law of which in the complex frequency domain is given by

$$V_{vref}(s)=V_0(s)+D_q\left(Q_{ref}(s)-Q(s)\right) \tag{2}$$

where V_0 is the normal magnitude of the grid phase voltage, and D_q is the droop coefficient of the Q-V droop control. $V_{vref}(s)$, $V_0(s)$, $Q_{ref}(s)$ and $Q(s)$ are the Laplace transformed variables of V_{vref}, V_0, Q_{ref} and Q, respectively.

B. Synchronous Resonance Analysis

In a rotating reference frame with the d axis aligned with $\mathbf{V_g}$, $\mathbf{V_{gdq}}$ and $\mathbf{v_{pdq}}$ are defined as the voltage vectors of $\mathbf{V_g}$ and $\mathbf{V_{pcc}}$ in dq-frame, which are thus expressed as

$$\mathbf{V_{gdq}}=V_g \quad \mathbf{v_{pdq}}=Ve^{j\delta} \tag{3}$$

where δ is defined as the power angle, representing the phase difference between $\mathbf{V_{pcc}}$ and $\mathbf{V_g}$, i.e., $\delta=\theta_{pcc}-\theta_g$. Then, the dynamics of the main circuit can be described in dq-frame as

$$L_g\frac{d\mathbf{i_{gdq}}}{dt}=\mathbf{v_{pdq}}-V_g-R_g\mathbf{i_{gdq}}-jX_g\mathbf{i_{gdq}} \tag{4}$$

Denoting the steady operating point in (3) and (4) with subscript "e", and the small-signal deviation added on the steady-state with a cap "^". Then linearizing (4) around the operating point, it is found that

$$\mathbf{V_{pdqe}}=V_e e^{j\delta_e} \quad \hat{\mathbf{v}}_{\mathbf{pdq}}=e^{j\delta_e}\left(\hat{v}+jV_e\hat{\delta}\right) \tag{5}$$

$$\mathbf{I_{gdqe}}=\frac{V_e e^{j\delta_e}-V_g}{R_g+jX_g} \tag{6}$$

$$L_g\frac{d\hat{\mathbf{i}}_{\mathbf{gdq}}}{dt}=\hat{\mathbf{v}}_{\mathbf{pdq}}-R_g\hat{\mathbf{i}}_{\mathbf{gdq}}-jX_g\hat{\mathbf{i}}_{\mathbf{gdq}} \tag{7}$$

By applying a Laplace transform to (7), yields

$$\hat{\mathbf{I}}_{\mathbf{gdq}}(s)=\frac{\hat{\mathbf{V}}_{\mathbf{pdq}}(s)}{sL_g+R_g+jX_g} \tag{8}$$

The complex power deviation can be expressed as

$$\hat{S}=1.5\left(\mathbf{V_{pdqe}}\hat{\mathbf{i}}^*_{\mathbf{gdq}}+\mathbf{I}^*_{\mathbf{gdqe}}\hat{\mathbf{v}}_{\mathbf{pdq}}\right)=\hat{P}+j\hat{Q} \tag{9}$$

where the superscript asterisk * denotes conjugation operator.

As in a high-voltage network, the inductance of the line impedance is much higher than the resistance. Thus the power coupling can be ignored, i.e., $\hat{P}$ is mainly determined by $\hat{\delta}$ and $\hat{v}$ affects $\hat{Q}$ a lot. Substituting (5), (6), and (8) into (9), the transfer functions from $\hat{P}(s)$ to $\hat{\delta}(s)$ and from $\hat{Q}(s)$ to $\hat{v}(s)$ can be derived as

$$G_{\delta p}(s)=\frac{\hat{P}(s)}{\hat{\delta}(s)}=\frac{-Q_e\left(sL_g+R_g\right)^2-Q_eX_g{}^2+1.5V_e{}^2X_g}{\left(sL_g+R_g\right)^2+X_g{}^2} \tag{10}$$

$$G_{vq}(s)=\frac{\hat{Q}(s)}{\hat{v}(s)}=\frac{\frac{Q_e}{V_e}\left(sL_g+R_g\right)^2+\frac{Q_e}{V_e}X_g{}^2+1.5V_eX_g}{\left(sL_g+R_g\right)^2+X_g{}^2} \tag{11}$$

From (10) and (11), it can be seen that $G_{\delta p}(s)$ and $G_{vq}(s)$

This article has been accepted for publication in a future issue of this journal, but has not been fully edited. Content may change prior to final publication. Citation information: DOI 10.1109/TIE.2021.3082055, IEEE Transactions on Industrial Electronics

contain a pair of conjugate poles, which are deduced as

$$p_{1,2} = -\frac{R_g}{L_g} \pm j\omega_0 \tag{12}$$

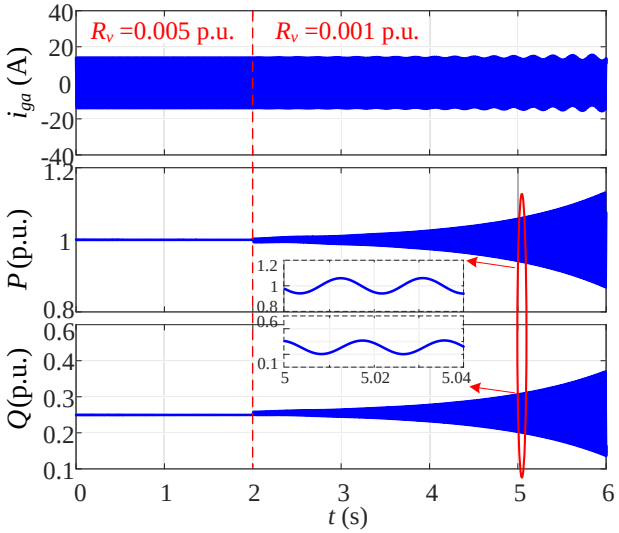

Fig. 2 Typical SR phenomena of the VSG with R_v is changed at 2s.

Thus, when R_g/X_g is very low, the poles will move closer to the imaginary axis. Consequently, the oscillation near the synchronous frequency ω_0 can be potentially triggered, which is the root cause of SR. Therefore, R_v is usually used to suppress the SR when R_g/X_g is very small. Fig. 2 shows the typical phenomena of the SR, which is triggered by decreasing R_v from 0.005 p.u. to 0.001 p.u. at 2s.

Based on the above analysis, it can be seen that R_v is inevitably adopted to damp the SR from a small-signal stability perspective. However, the effects of R_v on transient stability are still unknown, which should be further investigated.

III. Transient Stability Analysis When Considering Virtual Resistance

Generally, The dynamic performance of δ determines the transient stability of the VSG during the grid voltage sag studied in this paper. The transient stability is guaranteed if δ can be attracted to a stable steady-state value after the grid voltage sag. Otherwise, the system will lose stability if δ diverges to infinite.

Without the VR damping control, $V_{pcc} = V_{vref}$ and $\theta_{pcc} = \theta_{vref}$. Thus, P and Q, can be easily derived using V_{vref} and θ_{vref}. Combining with (2), V_{pcc} can be solved as a function of δ, and the relationship P-δ can be derived. However, when R_v is used, $\mathbf{V_{pcc}} = \mathbf{V_{ref}} = \mathbf{V_{vref}} - R_v\mathbf{I_g}$, which can be expressed with δ as follows

$$V_{pcc}e^{j\delta} = V_{vref}e^{j\theta_{vref}} - R_v \cdot \frac{V_{pcc}e^{j\delta} - V_g}{j\omega_0 L_g} \tag{13}$$

On the other hand, substituting Q into (2), V_{vref} can be deduced as the function of V_{pcc} and δ, i.e., V_{vref} (V_{pcc}, δ). Combining with (13), the intermediate variables V_{vref} and θ_{vref} should be eliminated to derive the relationship between V_{pcc} and δ, finally getting the P-δ relationship for transient stability analysis. But, due to the nonlinear trigonometric functions in (13), the explicit analytical expressions for $V_{pcc}(\delta)$ can not be solved. Thus, the P-δ relationship can not be obtained with an explicit mathematical analysis expression when R_v is adopted. To solve this problem, a virtual PCC is proposed in this paper for analyzing the effects of R_v on transient stability.

A. A Virtual PCC Proposed for Analyzing the Transient Response with R_v

The virtual PCC, which is equivalently derived from the control diagram, is before the real PCC, as shown in Fig. 3. The space vector of the virtual PCC voltage is denoted as $\mathbf{V_{vref}}$. The virtual power angle δ_{vir} is thus defined as $\delta_{vir} = \theta_{vref} - \theta_g$. The active and reactive power transmitted from the virtual PCC to the grid, denoted as P_{vir} and Q_{vir}, can be easily obtained. Then, the power injected into the grid from the real PCC, i.e., P and Q, can be derived by using P_{vir}, Q_{vir}, based on (14) and (15). Substituting (15) into (2), the relationship between V_{vref} and δ_{vir} can be derived, which is shown in (16). Note that (14), (15), and (16) are shown at the bottom of this page, where $R_{eq} = R_g + R_v$, K_X and K_R are

$$K_X = \frac{X_g}{R_{eq}^2 + X_g^2}, \quad K_R = \frac{R_{eq}}{R_{eq}^2 + X_g^2} \tag{17}$$

It should be noted that the power loss on R_v is not real, which is implemented in the control diagram and equivalently changes the power transmission.

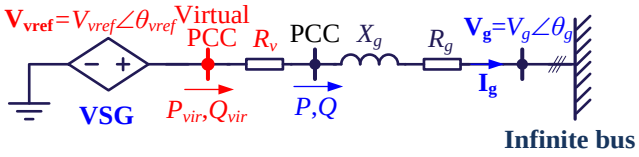

Fig. 3. Equivalent circuit of the VSG using virtual resistance damping.

$$P = P_{vir} - \frac{2}{3}\cdot\frac{\left(P_{vir}^2 + Q_{vir}^2\right)R_v}{V_{vref}^2} = \frac{3}{2}\cdot\frac{R_v\left(V_{vref}V_g\cos\delta_{vir} - V_g^2\right) + X_gV_{vref}V_g\sin\delta_{vir} + R_g\left(V_{vref}^2 - V_{vref}V_g\cos\delta_{vir}\right)}{R_{eq}^2 + X_g^2} \tag{14}$$

$$Q = Q_{vir} = \frac{3}{2}\cdot\frac{X_g\left(V_{vref}^2 - V_{vref}V_g\cos\delta_{vir}\right) - R_{eq}V_{vref}V_g\sin\delta_{vir}}{R_{eq}^2 + X_g^2} \tag{15}$$

$$V_{vref} = \frac{1.5K_XD_qV_g\cos\delta_{vir} + 1.5K_RD_qV_g\sin\delta_{vir} - 1 + \sqrt{\left(1.5K_XD_qV_g\cos\delta_{vir} + 1.5K_RD_qV_g\sin\delta_{vir} - 1\right)^2 + 6K_XD_q(V_0 + D_qQ_{ref})}}{3K_XD_q} \tag{16}$$

This article has been accepted for publication in a future issue of this journal, but has not been fully edited. Content may change prior to final publication. Citation information: DOI 10.1109/TIE.2021.3082055, IEEE Transactions on Industrial Electronics

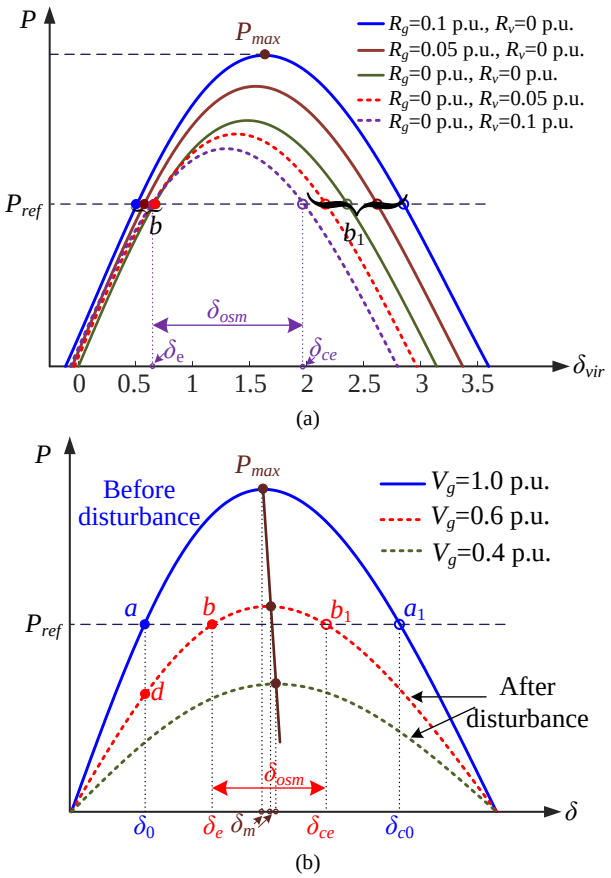

Fig. 4. P-δ_{vir} curves for (a) with different R_g and different R_v when V_g = 1.0 p.u., and (b) R_g = 0, R_v = 0 when the grid voltage drops. The other parameters are the same as given in Table I in Section V.

Substituting (16) to (14), the instantaneous relationship between P and the virtual power angle δ_{vir} can be obtained. The corresponding P-δ_{vir} curves with different VR and different grid resistors are plotted in Fig. 4(a). From there, it can be found that considering the impacts of the reactive power control loop, the effects of R_v and R_g on the active power transmission capability of the PCC are very different. The maximum power P_{max} that can be transmitted becomes higher with a larger R_g. However, P_{max} is reduced with a larger R_v.

To demonstrate the principle of transient instability, Fig. 4(b) illustrates the conceptual P-δ curves of the VSG with different grid voltage sags, where $\omega_g = \omega_0$ is assumed as the steady-state angular frequency after a disturbance for illustration convenience. There are two types of transient problems with different depths of grid voltage sag, i.e., the equilibrium point exists or not. According to IEEE Standards 1547-2018 [32], the VSG should continue to supply power at least for 10 s when the grid voltage drops to 0.5-0.8 p.u., indicating that the VSG should keep working normally during the fault for a long time. Therefore, this paper aims to promote the VSG to have equilibrium points and ride through the grid fault, as shown with the dashed red line in Fig. 4(b). There are two equilibrium points, i.e., b and b_1, representing the stable equilibrium point (SEP) and the unstable equilibrium point (UEP). The corresponding power angles are denoted as δ_e and δ_{ce}. During the transient period, the system should not go across b_1. Otherwise, it will lose synchronization with the grid, and δ will go beyond δ_{ce} and then go to infinite.

Therefore, $\delta_{osm} = \delta_{ce} - \delta_e$ is the maximum allowed power angle overshoot. If δ does not go beyond δ_{ce} during the transient period, the system can finally operate stably at point b.

From Fig. 4(a), it can be found that not only the effects of R_g and R_v on the active power transmission capability are different, but also on the variation range of the virtual power angle δ_{vir}. δ_{osm} is much larger with a larger R_g. However, the impacts of R_v are the opposite. The variation range of δ_{vir} is narrowed with a larger R_v. Although increasing R_g and R_v can both suppress the synchronous resonance, the influences on transient stability will be completely different. In practice, the performance of δ determines the VSG transient instability. Here, δ is replaced by the response of the virtual power angle δ_{vir}. From Fig. 4, it can also be found that although the power transmission capability varies with different R_g and R_v, all the P-δ_{vir} curves have a similar sinusoidal trend as the P-δ relationship without R_g and R_v in Fig. 4(b). P goes up first monotonously to P_{max} with the increase of δ_{vir}, and then monotonously declines to zero. The grid resistor R_g can benefit the transient performance due to that P_{max} is higher, and the maximum allowed power angle overshoot δ_{osm} is wider with R_g. Yet, increasing R_g will increase the power loss and reduce system efficiency. In order to suppress the synchronous resonance and avoid additional power loss, virtual resistance R_v is usually adopted. However, from Fig. 4, it can be concluded that adding R_v makes the transient performance worse. Since P_{max} is lower and δ_{osm} is narrowed with a larger R_v, it will jeopardize the transient power angle stability.

Remarks: it should be noted that the maximum power P_{max} in Fig. 4(a) is not the static power transfer limit which ignores the dynamic states and control strategy [33]. The power transfer capability in this paper is calculated according to the specific control strategy, which affects the modulation index, leading to different P-δ_{vir} curves obtained by using different virtual resistances.

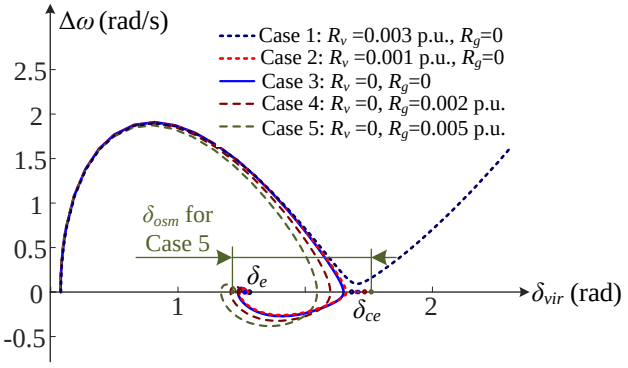

Fig. 5. The nonlinear system's phase portrait with different R_g and R_v when the grid voltage drops from 1 p.u. to 0.6 p.u.

B. The Transient Behaviors Based on the Phase Portrait

To figure out how the performances and responses are affected by using VR, the dynamic model needs to be established first. According to the previous analysis, it can be

This article has been accepted for publication in a future issue of this journal, but has not been fully edited. Content may change prior to final publication. Citation information: DOI 10.1109/TIE.2021.3082055, IEEE Transactions on Industrial Electronics

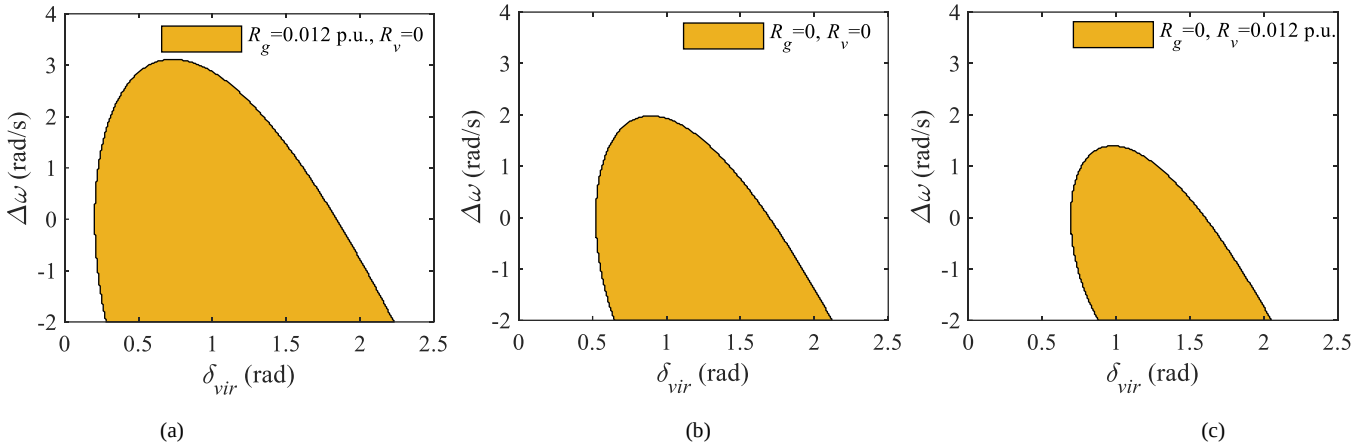

Fig. 6. Attraction region of the VSG with different R_g and R_v when the grid voltage drops to 0.6 p.u., (a) R_g = 0.012 p.u., R_v =0; (b) R_g = 0, R_v =0; (c) R_g = 0, R_v =0.012 p.u..

known that the system is a second-order nonlinear system. The dynamic response of the virtual power angle can be represented in the standard form as

$$\begin{bmatrix} \dot{\delta}_{vir} \\ \Delta\dot{\omega} \end{bmatrix} = \begin{bmatrix} \Delta\omega + \omega_0 - \omega_g \\ -\frac{D_p}{J}\Delta\omega - \frac{P(\delta_{vir})}{J} + \frac{P_{ref}}{J} \end{bmatrix} \tag{18}$$

where dot (·) denotes time derivative, and $P(\delta_{vir})$ is shown in (14).

By setting all the differential items, i.e., the left terms in (18), to zero, the equilibrium point $\boldsymbol{x_e} = [\delta_{vire}, \Delta\omega_e]^T$ can be derived. This implies $\Delta\omega_e = \omega_g - \omega_0$, and δ_{vire} should satisfy that

$$P(\delta_{vire}) = P_{ref} - D_p\left(\omega_g - \omega_0\right) \tag{19}$$

The influence of R_g and R_v on the transient behavior is illustrated in Fig. 5 based on the phase portrait of the system in (18). It can clearly be observed that increasing R_v narrows the allowable range for the overshoot of δ_{vir}. As a result, the peak power angle during the transient period is more closed to the UEP or even goes beyond it and causes instability. Such as a larger R_v, i.e., R_v = 0.003 p.u., can cause the loss of synchronization with the grid, even when the equilibrium points exist. In contrast, a larger R_g can broaden the allowable range for the overshoot of δ_{vir}, leading to a peak power angle much smaller than the UEP during the transient period, enhancing the transient stability of the system.

The phase portrait showed the performances of the virtual power angle and frequency changes during the grid voltage sag. However, it is just based on one initial condition, which cannot predict and analyze what will happen with different initial states. Thus, the attraction region with the different initial states is also derived in Fig. 6 to investigate the effects of R_g and R_v further. If the initial state belongs to the attraction region, the VSG will be stable after the grid voltage drops to 0.6 p.u.. From Fig. 6, it can clearly be observed that the attraction region can be expanded with the increase of R_g but reduced by adding R_v, which verifies that R_v has negative impacts on the transient stability.

Obviously, there is a conflict by adding R_v. When the parasitic R_g in the circuit is too small, especially in the high-voltage power grid, adding R_v is necessary to suppress the synchronous resonance. However, R_v is unexpected from a transient stability perspective. Therefore, there is an urgent demand to weaken the effects of R_v on transient stability.

IV. Reducing the Active Power Reference to Enhance Transient Stability

A. *Effect of Power Reference During the Grid Voltage Sag*

From the analysis mentioned above, the main cause for the transient instability is the large virtual power angle overshoot with narrowed allowable range while R_v is adopted. Thus, a natural ideal for stability enhancement is to broaden the allowable range of δ_{vir}, which can be easily achieved by reducing the active power reference when the grid voltage drops, as shown in Fig. 7. Once grid fault occurs, P_{ref} is reduced to P_{refn}, the SEP and UEP are thus changed from b, b_1 to b_n, b_{1n}, respectively. As a consequence, the allowable overshoot range of δ_{vir}, i.e., δ_{osmn}, is much wider than the original one δ_{osm}, which can effectively enhance the transient stability.

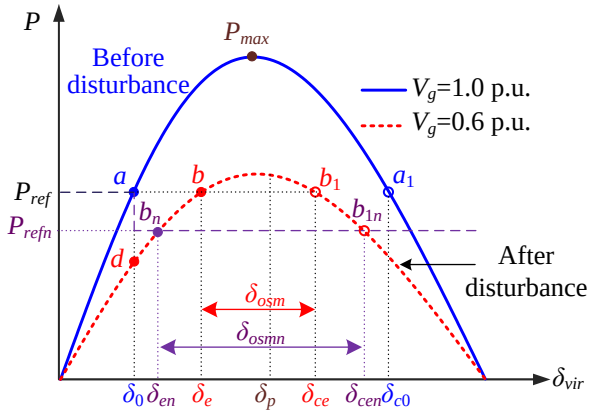

Fig. 7. The diagram of P-δ_{vir} curves with reduced active power reference when grid voltage drops.

This article has been accepted for publication in a future issue of this journal, but has not been fully edited. Content may change prior to final publication. Citation information: DOI 10.1109/TIE.2021.3082055, IEEE Transactions on Industrial Electronics

B. *Design of Power Reference During Grid Voltage Sag*

Although reducing the active power reference during the transient period is effective, detecting the grid fault and how to design P_{refn}, need to be discussed further.

Since the transient problems are caused by grid voltage sag, which also leads to a voltage drop on V_{pcc} (so as V_{vref}), thus, V_{pcc} (or V_{vref}) can be used to detect whether the grid voltage sag occurs. Fig. 8 shows the normal values of V_{vref} with different power requirements. From there, it can be seen that V_{vref} will increase when Q_{ref} increases, which can help improve the transient behaviors. However, V_{vref} declines with a larger active power requirement. The worst case is that V_{vref} decreases to 0.977 p.u. when Q_{ref} = 0, P_{ref} = 1 p.u. without R_g and R_v. If R_g and R_v are considered, the minimum V_{vref} rises a bit at the normal operation. In order to keep a margin, the threshold voltage level of detecting the grid voltage sag is setting at 0.95 p.u., i.e., V_{vrefth} = 0.95 p.u.. Once V_{vref} <= V_{vrefth} is detected, indicating the grid voltage sag occurs, a power reduction, which is related to the voltage drop, is introduced to the active power reference, as shown in Fig. 9. There is a switch, i.e., k, which is 1 when the grid fault is detected. If V_{vref} > V_{vrefth}, k =0, then the additional path does not affect the normal operation. It should be noted that increasing Q_{ref} can also enhance the transient stability when a voltage sag occurs. However, P_{ref} should be reduced simultaneously due to the grid-connected converter's limited capacity in reality. There is a rated apparent power for each converter, which cannot be exceeded. Therefore, increasing Q_{ref} and decreasing P_{ref} should be combined and optimized together, which is worthy of more in-depth study.

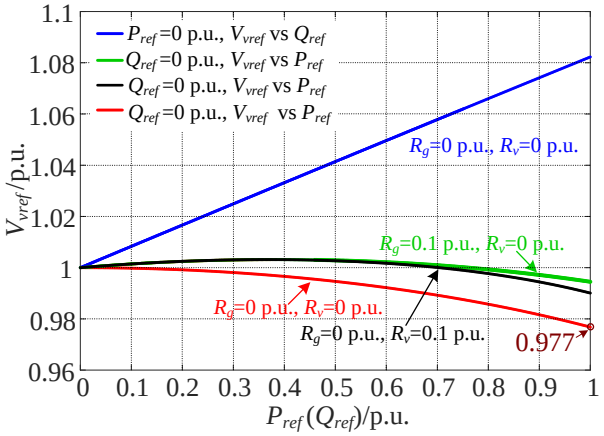

Fig. 8. The values of V_{vref} with different power requirements under normal grid voltage.

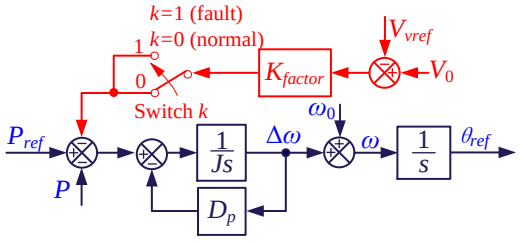

Fig. 9. Block diagram of the active power control loop with P_{ref} reduction during the grid voltage sag.

From Fig. 9, the dynamic of the second-order nonlinear system is changed differently from (18), which can be derived as

$$\begin{bmatrix} \dot{\delta}_{vir} \\ \Delta\dot{\omega} \end{bmatrix} = \begin{bmatrix} \Delta\omega + \omega_0 - \omega_g \\ -\frac{D_p}{J}\Delta\omega - \frac{P(\delta_{vir})}{J} + \frac{P_{ref}}{J} - \frac{K_{factor}\left(V_0 - V_{vref}(\delta_{vir})\right)}{J} \end{bmatrix} \quad (20)$$

where $P(\delta_{vir})$ and $V_{vref}(\delta_{vir})$ are shown in (14) and (16), respectively.

From Fig. 9 and (20), we can know that the coefficient K_{factor} is the key factor for enhancing transient stability. Thus, it is an important issue to design this factor. According to (20), the transient behaviors with the method of reducing P_{ref} are illustrated in Fig. 10 by using the phase portrait. It can be observed that without the additional power reduction path, instability occurs when the grid voltage drops from 1 p.u. to 0.6 p.u. with R_v = 0.015 p.u.. In the same case, the instability can be avoided by increasing the coefficient factor K_{factor}, due to the enlarged allowable range of δ_{vir}. Otherwise, instability can occur if K_{factor} is not large enough, i.e., K_{factor} = 0.5. Furthermore, as can be seen from the figure, the maximum frequency deviation $\Delta\omega_{max}$ is decreased a lot for case 5 compared with case 1. This means the proposed control strategy can also reduce the frequency deviations during the grid voltage sags, which benefits the frequency stability during the transient period.

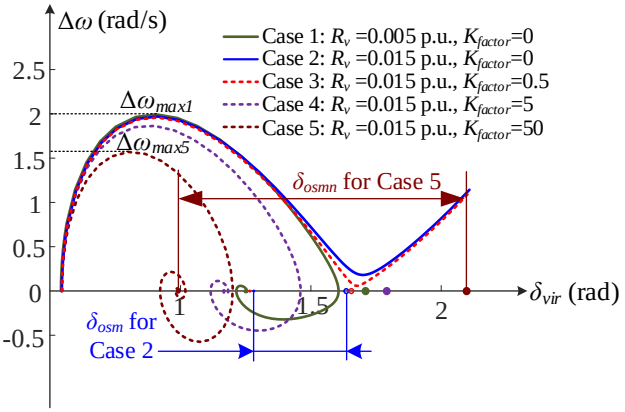

Fig. 10. The influence of parameters K_{factor} on the phase portrait of the VSG with R_g = 0.003 p.u. when V_g = 1→ 0.6 p.u..

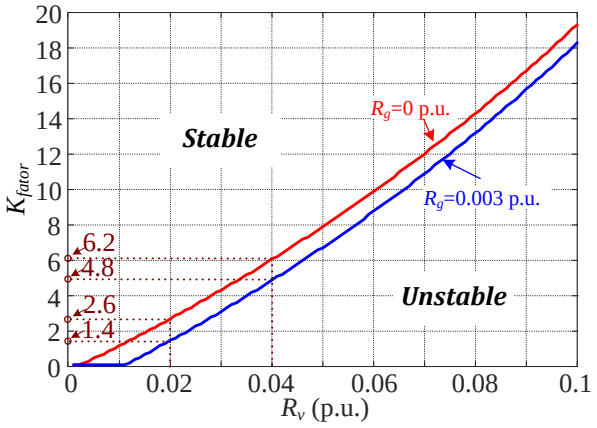

Fig. 11. The required K_{factor} for specified R_g and R_v when V_g = 1→ 0.6 p.u.

This article has been accepted for publication in a future issue of this journal, but has not been fully edited. Content may change prior to final publication. Citation information: DOI 10.1109/TIE.2021.3082055, IEEE Transactions on Industrial Electronics

Although a larger K_{factor} is beneficial for transient stability, it will also reduce the transferred active power more. According to IEEE Standards 1547-2018 [24], the VSG should keep providing power normally for a long time when the grid voltage drops to 0.5-0.8 p.u. Thus, too large K_{factor} can not be accepted. How to obtain a critical K_{factor} for a specified R_v is urgently needed. Using Matlab command "ode45" to solve the nonlinear state equations in (20) by sweeping K_{factor} from a large value to a small one with a tiny calculation step, the critical value can be obtained. The procedure was then repeated to find all critical values of K_{factor} under different R_g and R_v settings, as shown in Fig.11, where the stable and unstable regions of operation are located above and below the boundary line, respectively. It can be seen that the minimum required K_{factor} for the stable operation increases with the increase of R_v. Meanwhile, a larger R_g can make the minimum required K_{factor} decline. For example, if R_v = 0.02 p.u, K_{factor} > 1.4 is required when R_g = 0.003 p.u., but K_{factor} > 2.6 must be adopted for R_g = 0 p.u.

It is worth noting that the analysis methodology for a transient issue and the stability assessment in this paper can be applied to the other types of grid disturbances using a similar procedure. The enhancement method for transient stability is also effective during other types of grid faults, such as a grid impedance change. There is another concern about the power balance when decreasing the active power reference during the grid faults. However, it should be noted that the power balance is not maintained by one converter at the fault side, which is usually achieved by secondary or tertiary control from a systematic view. In this paper, only the primary control of the converter is mainly focused on and studied during the grid faults. Thus, the detailed power balance issue during grid faults is out of the scope of this paper.

V. Experimental Verification

To verify the theoretical analysis for the effects of the VR on transient stability, meanwhile, to validate the improved method of reducing the active power reference, experiments are carried out with a three-phase grid-connected converter. The experimental setup is shown in Fig. 12. A constant dc voltage supply provides the input dc voltage, and a Chroma grid simulator is employed to emulate the infinite bus. The dSPACE DS1007 platform is used to implement the control strategies, where the needed voltage and current are measured by the dSPACE DS2004 A/D board. The calculated active power and the power angle are transmitted to the oscilloscope through the DS2102 D/A board. For example, the phase angles of $\mathbf{V_{pcc}}$ and $\mathbf{V_g}$ are measured by two PLLs in the dSPACE DS1007 platform, denoting as θ_{pcc} and θ_g. Then, the power angle is $\delta = \theta_{pcc} - \theta_g$ is calculated, which is further transmitted to the oscilloscope through the DS2102 D/A board.

The main parameters of the VSG are presented in Table I, where a low voltage and power level were intentionally chosen for the convenience of establishing an experimental setup. SCR is set at 2 to emulate a weak grid. Thus, the grid inductance is calculated as 12 mH. D_p and D_q are the droop coefficients selected according to the grid codes, like in [25]. A large virtual inertia J is designed to satisfy the allowed RoCoF requirement [7], [25]. Firstly, the transient behaviors of the VSG under the grid voltage drops from 1 p.u. to 0.6 p.u. are tested in Fig. 13 and Fig. 14. From top to bottom in each picture, the corresponding experimental waveforms are the grid line-voltage, i.e., V_{gab}, the active power P, power angle δ, and the line current of phase a, I_{ga}, respectively.

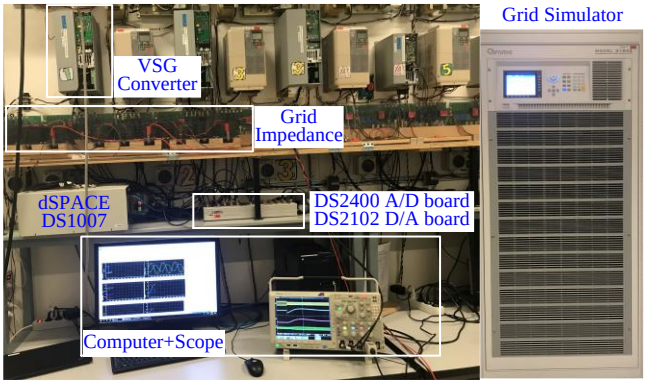

Fig.12. The hardware platform used in the experiments to validate the theoretical analysis.

TABLE I
Main Parameters of the VSG System Used in Experiments

Parameters	Description	Value	p.u.
P_{ref}	Rated active power	2 kW	1.0
Q_{ref}	Rated reactive power	0	0
V_0	Rated voltage	100 V	1.0
V_g	Normal grid voltage	100 V	1.0
ω_0	Grid angular frequency	314 rad/s	1.0
L_g	Grid inductance	12 mH	0.5
R_g	Equivalent grid resistance	22.5 mΩ	0.003
D_p	*P-f* droop gain	25 P_{max}/ω_0	25
J	Virtual inertia	10 P_{max}/ω_0	10
D_q	*Q-V* droop gain	0.1V_0/Q_{max}	0.1

In Fig.13, when R_v = 0.005 p.u. is adopted, the system can return to the stable steady-state when V_g drops from 1 p.u. to 0.6 p.u.. However, if R_v is increased to 0.015 p.u., the system becomes unstable, and a low-frequency oscillation is observed when the fault is triggered. This implies that instability is caused by the narrowed allowable overshoot range of δ. The results validate the theoretical analysis for the effects of R_v on the transient stability in Fig. 4.

In Fig.14, a reduction of the active power reference during the grid voltage sag is performed to enhance the transient stability with different coefficient parameters settings. From Fig. 14(a), it can be found that the method of reducing P_{ref} with a large coefficient K_{factor} can stabilize the VSG when the grid voltage drops. However, if K_{factor} is not large enough, i.e., K_{factor} = 0.2, the transient instability still exists. The results agree with the theoretical analysis of the improved method of reducing the active power reference shown in Fig. 10 and Fig. 11, respectively.

To further validate the improved method for transient stability, Fig. 15 shows the transient waveforms for the grid voltage drops from 1 p.u. to 0.4 p.u.. If P_{ref} keeps constant like that before the fault or K_{factor} is too small, there will be no equilibrium point. The system definitely loses its stability,

This article has been accepted for publication in a future issue of this journal, but has not been fully edited. Content may change prior to final publication. Citation information: DOI 10.1109/TIE.2021.3082055, IEEE Transactions on Industrial Electronics

which can not be removed even if the fault was cleared, as shown in Fig. 15(a). Nevertheless, if K_{factor} is sufficiently large, i.e., K_{factor} = 50 in Fig. 15(b), the system can operate stably during the fault. Moreover, the system can return to the original state when the fault was cleared as long as it is stable during the fault. These experimental results further validate the effectiveness of the enhanced method for the transient stability.

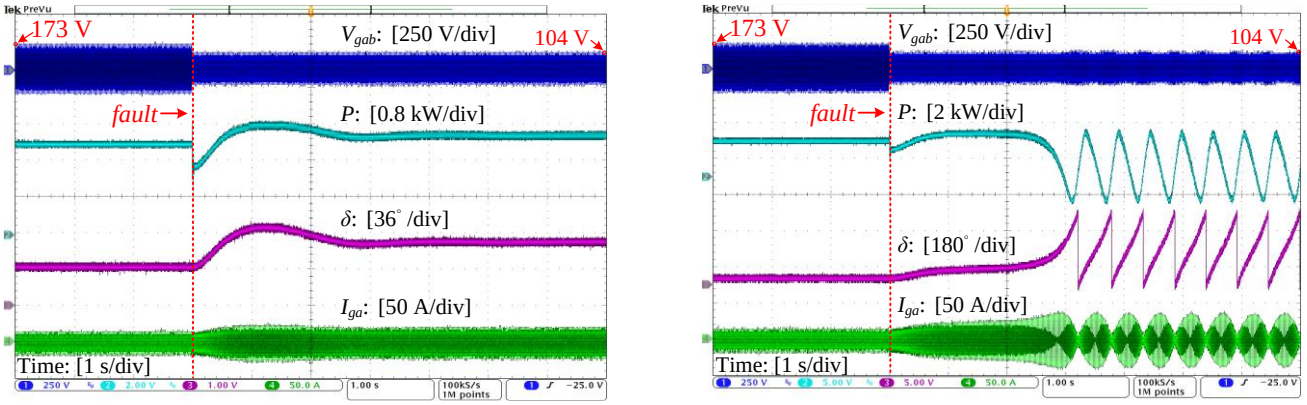

(a) (b)

Fig. 13. Experimental transient responses of the VSG with different R_v when V_g drops from 1 p.u. to 0.6 p.u. (a) R_v = 0.005 p.u. and (b) R_v = 0.015 p.u..

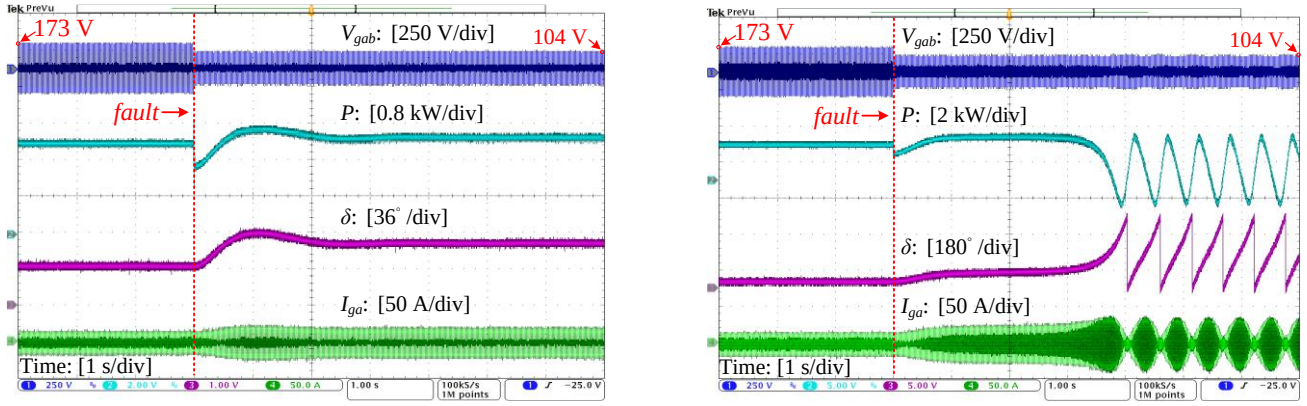

(a) (b)

Fig. 14. Experimental transient responses of the VSG with R_v = 0.015 p.u. when V_g dips from 1 p.u. to 0.6 p.u. The improved method of reducing active power reference are added with different coefficients, (a) K_{factor} = 5, (b) K_{factor} = 0.2.

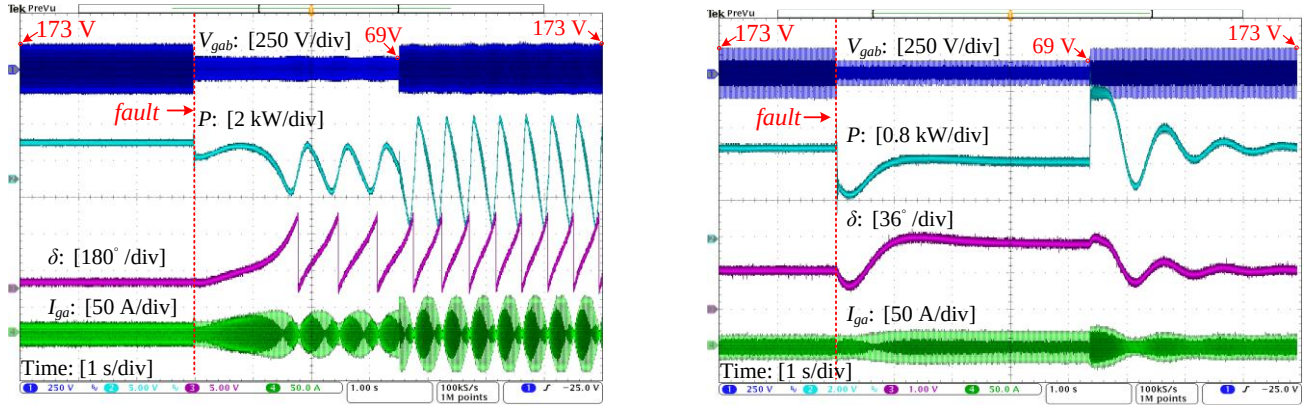

(a) (b)

Fig. 15. Experimental transient behaviors of the VSG with R_v = 0.015 p.u. when V_g dips from 1 p.u. to 0.4 p.u. The improved method of reducing active power reference is added with different coefficients, (a) K_{factor} = 20, (b) K_{factor} = 50.

VI. Conclusion

The effects of VR on transient stability are first studied in this paper. A virtual PCC and a virtual power angle are proposed to represent the mathematical model of the VSG with VR damping. Based on that, transient stability is analyzed using the phase portrait and the attraction regions of the system. It reveals that the impacts of VR on transient stability are opposite from the grid resistance, which narrowed the stability region of the VSG, resulting from reducing the active power transfer capability. In

order to keep the VSG with VR work normally during the grid voltage sag, an enhanced transient stability method, by reducing the active power reference as the grid fault is detected, is introduced. A design-oriented analysis and the parameter design with different VRs are also presented, indicating that a more considerable reduction on active power reference is required with a larger VR during the grid fault. Finally, experimental results have verified the effectiveness of the theoretical analysis and the enhanced method for transient stability.

REFERENCES

[1] F. Blaabjerg, R. Teodorescu, M. Liserre, and A. V. Timbus, "Overview of control and grid synchronization for distributed power generation systems," *IEEE Trans. Ind. Electron.*, vol. 53, no. 5, pp. 1398−1409, Oct. 2006.

[2] L. Harnefors, X. Wang, A. Yepes, and F. Blaabjerg, "Passivity-based stability assessment of grid-connected VSCs - an overview," *IEEE Jour. Emer. Select. Top. Power Electron.*, vol. 4, no. 1, pp. 116-125, Mar. 2016.

[3] D. Dong, B. Wen, D. Boroyevich, P. Mattavelli, and Y. Xue, "Analysis of phase-locked loop low-frequency stability in three-phase grid-connected power converters considering impedance interactions," *IEEE Trans. Ind. Electron.*, vol. 62, no. 1, pp. 310–321, Jan. 2015.

[4] J. M. Guerrero, P. C. Loh, M. Chandorkar, and T.-L. Lee, "Advanced control architectures for intelligent microgrids, part I: Decentralized and hierarchical control," *IEEE Trans. Ind. Electron.*, vol. 60, no. 4, pp. 1254–1262, Apr. 2013.

[5] Y. Deng, Y. Tao, G. Chen, G. Li, and X. He, "Enhanced power flow control for grid-connected droop-controlled inverters with improved stability," *IEEE Trans. Ind. Electron.*, vol. 64, no. 7, pp. 5919−5929, July 2017.

[6] J. Quintero, V. Vittal, G. T. Heydt, and H. Zhang, "The impact of increased penetration of converter control-based generators on power system modes of oscillation," *IEEE Trans. Power Syst.*, vol. 29, no. 5, pp. 2248–2256, Sep. 2014.

[7] J. Fang, H. Li, Y. Tang and F. Blaabjerg, "On the inertia of future more-electronics power systems," *IEEE J. Emerg. Sel. Topics Power Electron.*, vol. 7, no. 4, pp. 2130-2146, Dec. 2019.

[8] S. D. Arco, J. A. Suul, and O. B. Fosso, "A virtual synchronous machine implementation for distributed control of power converters in SmartGrids," *Electr. Power Syst. Res.*, vol. 122, pp. 180−197, May 2015.

[9] D. Chen, Y. Xu, and A. Q. Huang, "Integration of dc microgrids as virtual synchronous machines into the ac grid," *IEEE Trans. Ind. Electron.*,vol. 64, no. 9, pp. 7455–7466, Sep. 2017.

[10] S. A. Khajehoddin, M. Karimi-Ghartemani, and M. Ebrahimi, "Grid supporting inverters with improved dynamics," *IEEE Trans. Ind. Electron.*, vol. 66, no. 5, pp. 3655–3667, May 2019.

[11] Y. Chen, R. Hesse, D. Turschner et al., "Dynamic properties of the virtual synchronous machine (VISMA)," *Renew. Energy Power Qual. J.*, vol. 1, no. 9, pp. 755-759, May 2011.

[12] Q. C. Zhong and G. Weiss, "Synchronverters: inverters that mimic synchronous generators," *IEEE Trans. Ind. Electron.*, vol. 58, no. 4, pp. 1259−1267, Apr. 2011.

[13] C. Yang, L. Huang, H. Xin, and P. Ju, "Placing grid-forming converters to enhance small signal stability of PLL-integrated power systems," *IEEE Trans. Power Syst.*, early access, 2020

[14] L. Huang, H. Xin, H. Yang, Z. Wang, and H. Xie, "Interconnecting very weak AC systems by multiterminal VSC-HVDC links with a unified virtual synchronous control," *IEEE J. Emerg. Sel. Topics Power Electron.*, vol. 6, no. 3, pp. 1041-1053, Sept. 2018.

[15] W. Wang, L. Jiang, Y. Cao, and Y. Li, "A parameter alternating VSG controller of VSC-MTDC systems for low frequency oscillation damping," *IEEE Trans. Power Syst.*, vol. 35, no. 6, pp. 4609-4621, Nov. 2020.

[16] L. Huang, H. Xin and Z. Wang, "Damping low-frequency oscillations through VSC-HVDC stations operated as virtual synchronous machines," *IEEE Trans. Power Electron.*, vol. 34, no. 6, pp. 5803-5818, June 2019.

[17] G. Li, Y. Chen, A. Luo, Z. He, H. Wang, Z. Zhu, and L. Zhou, "Analysis and mitigation of subsynchronous resonance in series-compensated grid-connected system controlled by a virtual synchronous generator," *IEEE Trans. Power Electron.*, vol. 35, no. 10, pp. 11096-11107, Oct. 2020.

[18] G. Li, Y. Chen, A. Luo, and H. Wang, "An enhancing grid stiffness control strategy of STATCOM/BESS for damping sub-synchronous resonance in wind farm connected to weak grid," *IEEE Trans. Industr. Inform.*, vol. 16, no. 9, pp. 5835-5845, Sept. 2020.

[19] L. Zhang, L. Harnefors, and H.-P. Nee, "Power-synchronization control of grid-connected voltage-source converters," *IEEE Trans. Power Syst.*,vol. 25, no. 2, pp. 809–920, May 2010.

[20] J. Wang, Y. Wang, Y. Gu, W. Li, and X. He, "Synchronous frequency resonance of virtual synchronous generators and damping control". in *Proc. IEEE Energy Convers. Congr. Expo.*, 2015, pp. 1011–1016.

[21] L. Harnefors, M. Hinkkanen, U. Riaz, F. M. M. Rahman and L. Zhang, "Robust Analytic Design of Power-synchronization control," *IEEE Trans. Ind. Electron*, vol. 66, no. 8, pp. 5810–5819, August 2019.

[22] D. Yang, H. Wu, X. Wang, and F. Blaabjerg, "Suppression of synchronous resonance for VSGs," in *J. Eng.*, vol. 2017, no. 13, pp. 2574-2579, 2017.

[23] D. Yang, X. Wang and F. Blaabjerg, "Fast power control for VSCs to enhance the synchronization stability in ultra-weak grids," *2018 IEEE Power & Energy Society General Meeting (PESGM)*, Portland, OR, pp. 1-6, 2018.

[24] J. Rocabert, A. Luna, F. Blaabjerg, and P. Rodríguez, "Control of power converters in ac microgrids," *IEEE Trans. Power Electron.*, vol. 27, pp. 4734–4749, Nov 2012.

[25] D. Pan, X. Wang, F. Liu and R. Shi, "Transient Stability of Voltage-Source Converters with Grid-Forming Control: A Design-Oriented Study," *IEEE J. Emerg. Sel. Topics Power Electron.*, vol. 8, no. 2, pp. 1019- 1033, June 2020.

[26] H. Cheng, Z. Shuai, C. Shen, X. Liu, Z. Li and Z. J. Shen, "Transient angle stability of paralleled synchronous and virtual synchronous generators in islanded microgrids," *IEEE Trans. Power Electron.*, vol. 35, no. 8, pp. 8751-8765, Aug. 2020.

[27] H. Wu and X. Wang, "A mode-adaptive power-angle control method for transient stability enhancement of virtual synchronous generators," *IEEE J. Emerg. Sel. Topics Power Electron.*, vol. 8, no. 2, pp. 1034- 1049, Jun. 2020.

[28] T. Liu and X. Wang, "Transient stability of single-loop voltage-magnitude controlled grid-forming converters," *IEEE Trans. Power Electron., early access*, 2020.

[29] X. Wang, M. G. Taul, H. Wu, Y. Liao, F. Blaabjerg, and L. Harnefors, "Grid-synchronization stability of converter-based resources—an overview," in *IEEE Open J. Ind. Appl.*, vol. 1, pp. 115-134, 2020.

[30] P. Pan, W. Chen, L. Shu, H. Mu, K. Zhang, M. Zhu, F. Deng, "An impedance-based stability assessment methodology for DC distribution power system with multivoltage levels," *IEEE Trans. Power Electron.*, vol. 35, no. 4, pp. 4033-4047, April 2020.

[31] J. Zhao, M. Huang, H. Yan, C. K. Tse and X. Zha, "Nonlinear and transient stability analysis of phase locked loops in grid-connected converters," *IEEE Trans. Power Electron.*, vol. 36, no. 1, pp. 1018- 1029, Jan. 2021.

[32] "IEEE standard for interconnection and interoperability of distributed energy resources with associated electric power systems interfaces," in IEEE Std 1547-2018 (Revision of IEEE Std 1547-2003) , vol., no., pp.1-138, 6 April 2018.

[33] J. A. Suul, S. D'Arco, P. Rodriguez, and M. Molinas, "Impedance-compensated grid synchronization for extending the stability range of weak grids with voltage source converters," IET Gener., Trans. Distr., vol. 10, no. 6, pp. 1315-1326, Apr. 2016.

Xiaoling Xiong (M'19) received the B.S., M.S. and Ph.D degrees in electrical engineering from Nanjing University of Aeronautics and Astronautics, Nanjing, China, in 2007, 2010 and 2015 respectively. She had worked as a Research Assistant in Department of Electronic and Information Engineering at Hong Kong Polytechnic University from February, 2011 to July, 2012.

Since 2015, she has been with North China Electric Power University, Beijing, where she was a lecturer. Simultaneously, she has been with Aalborg University, Aalborg, Denmark from December, 2018 to November, 2020, where she was a visiting Post-Doctoral with the Department of Energy Technology. Her current research interests include HVDC system, modeling, analysis and design power electronic systems and study the nonlinear behaviors in power electronic circuits.

This article has been accepted for publication in a future issue of this journal, but has not been fully edited. Content may change prior to final publication. Citation information: DOI 10.1109/TIE.2021.3082055, IEEE Transactions on Industrial Electronics

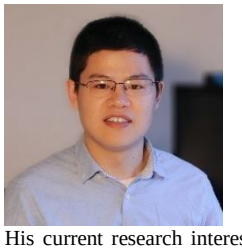

Chao Wu (M'19) was born in Hubei Province, China. He received the B.Eng. degree from HeFei University of Technology, Hefei, China and the Ph.D. degree from Zhejiang University, Hangzhou, China, in 2014 and 2019, both in electrical engineering. He is currently a Postdoctoral Researcher in the Department of Energy Technology, Aalborg University, Aalborg, Denmark.

His current research interests include cooperative control of multi-converter systems, particularly the control and operation of doubly fed induction generators for DC connection and the transient stability of power converters.

Frede Blaabjerg (S'86–M'88–SM'97–F'03) was with ABB-Scandia, Randers, Denmark, from 1987 to 1988. From 1988 to 1992, he got the PhD degree in Electrical Engineering at Aalborg University in 1995. He became an Assistant Professor in 1992, an Associate Professor in 1996, and a Full Professor of power electronics and drives in 1998. From 2017 he became a Villum Investigator. He is honoris causa at University Politehnica Timisoara (UPT), Romania and Tallinn Technical University (TTU) in Estonia.

His current research interests include power electronics and its applications such as in wind turbines, PV systems, reliability, harmonics and adjustable speed drives. He has published more than 600 journal papers in the fields of power electronics and its applications. He is the co-author of four monographs and editor of ten books in power electronics and its applications.

He has received 32 IEEE Prize Paper Awards, the IEEE PELS Distinguished Service Award in 2009, the EPE-PEMC Council Award in 2010, the IEEE William E. Newell Power Electronics Award 2014, the Villum Kann Rasmussen Research Award 2014, the Global Energy Prize in 2019 and the 2020 IEEE Edison Medal. He was the Editor-in-Chief of the IEEE TRANSACTIONS ON POWER ELECTRONICS from 2006 to 2012. He has been Distinguished Lecturer for the IEEE Power Electronics Society from 2005 to 2007 and for the IEEE Industry Applications Society from 2010 to 2011 as well as 2017 to 2018. In 2019-2020 he serves a President of IEEE Power Electronics Society. He is Vice-President of the Danish Academy of Technical Sciences too.

He is nominated in 2014-2019 by Thomson Reuters to be between the most 250 cited researchers in Engineering in the world.